Investigation of the Diffusion Region With Varying Turbulence Intensities Around the X-Line of Magnetotail Reconnection

Xinmin Li[1,2] , Rongsheng Wang[1,3,4] , Chuanfei Dong[5] , Quanming Lu[1,3,4] , San Lu[1,3,4] , Julia E. Stawarz[6] , Yi Qi[7] , Liang Wang[5], and J. L. Burch[8]

[1]Deep Space Exploration Laboratory/School of Earth and Space Sciences, University of Science and Technology of China, Hefei, China, [2]Now at Center for Space Physics and Department of Astronomy, Boston University, Boston, MA, USA, [3]CAS Center for Excellence in Comparative Planetology/CAS Key Laboratory of Geospace Environment/Anhui Mengcheng National Geophysical Observatory, University of Science and Technology of China, Hefei, China, [4]Collaborative Innovation Center of Astronautical Science and Technology, Harbin, China, [5]Center for Space Physics and Department of Astronomy, Boston University, Boston, MA, USA, [6]Department of Mathematics, Physics and Electrical Engineering, Northumbria University, Newcastle Upon Tyne, UK, [7]Laboratory for Atmospheric and Space Physics, Boulder, CO, USA, [8]Southwest Research Institute, San Antonio, TX, USA

Abstract Magnetic reconnection and turbulence are two fundamental processes in space plasma environments. They are intricately coupled, driving energy transfer and conversion. Despite significant research efforts, the development of turbulence within the reconnection diffusion region and its impact on the reconnection process remain open questions. In this study, we analyze 16 magnetotail reconnection cases observed by the Magnetospheric Multiscale (MMS) mission, focusing on the diffusion regions in the vicinity of the X-line. We find that turbulence tends to be stronger in diffusion regions with lower plasma density and plasma beta. Turbulence can enhance the electron energization process in the diffusion region primarily through electron heating. As turbulence intensifies, the continuous current layer of the diffusion region breaks into fragmented currents, suggesting a transition from laminar to turbulent reconnection. Moreover, spectral breaks between ion and electron cyclotron frequencies are consistently observed in magnetic and electric field fluctuations within reconnecting current sheets, suggesting that such breaks may be a characteristic feature of the reconnection process. These findings provide valuable insights into the development and role of turbulence within the reconnection diffusion region.

Plain Language Summary Magnetic reconnection is a common process in space plasma environments that releases magnetic energy, heating the plasma and accelerating particles. Turbulence, another ubiquitous phenomenon, transfers energy from large to small scales. These two processes are often closely related: reconnection occurs more readily in turbulent plasmas, facilitating energy cascade and dissipation; meanwhile, turbulence can develop within the reconnecting current sheet and, in turn, influence the underlying physical processes. In this study, we focus on how turbulence develops and affects the physical processes inside the reconnection diffusion region. Our results show that turbulence develops more easily in the reconnecting current sheet when the plasma density and plasma beta are lower. As turbulence increases, the current sheet of the diffusion region breaks into tiny patchy currents. Moreover, turbulence can further enhance electron energization within the diffusion region. We also find that spectral breaks between ion and electron cyclotron frequencies are consistently observed in magnetic and electric field fluctuations within reconnecting current sheets, suggesting that such breaks may be a characteristic feature of the reconnection process. These findings help us better understand how magnetic reconnection and turbulence interact in the space plasma environment.

1. Introduction

Magnetic reconnection is a fundamental physical process that reconfigures the topology of magnetic field lines and releases magnetic energy to heat plasmas and accelerate particles in space and astrophysical plasma environments (Ji et al., 2022; Lu et al., 2022). The diffusion region is the most important region of magnetic reconnection, in which the magnetic field lines "break" and "reconnect", leading to the dissipation of the magnetic energy. In collisionless plasma environments, the diffusion region is a multi-scale structure comprising an ion diffusion region (IDR) and an embedded electron diffusion region (EDR) (Fu et al., 2006; Hesse et al., 1999;

Pritchett, 2001; Shay et al., 1998). The IDR thickness is on the ion-scale leading to the decoupling of the ions from the magnetic field lines. The relative motions between ions and electrons result in the Hall effects, which effectively increase the reconnection rate (Deng & Matsumoto, 2001; Lu et al., 2010; Ma & Bhattacharjee, 2001; Oieroset et al., 2001; Wang et al., 2015, 2017). The EDR is an electron-scale current layer located around the X-line where ion outflow reversal occurs. Inside the EDR, both the electrons and ions are decoupled from magnetic fields. This region is always associated with intense energy conversion rate and crescent-shaped electron velocity distributions (Burch et al., 2016; Li et al., 2019; Shay et al., 2016; Torbert et al., 2018; Wang, Lu, et al., 2020; Webster et al., 2018; Zenitani et al., 2011; Zhou et al., 2019a).

Recent observations, however, suggest that the structure of the EDR can be more complex. Sometimes, the EDRs display bifurcation structures consisting of multiple current sub-layers instead of an intact current layer (Cozzani et al., 2021; Genestreti et al., 2022; Liu et al., 2013; Tang et al., 2022; Wang et al., 2023). More recently, our previous observations show that the EDR could fragment into a 3D filamentary current network (Li, Wang, Lu, et al., 2022). The complex structure of the EDR suggests that it has developed into a turbulent state. Several possible mechanisms for such development of turbulence inside the EDR have been proposed, such as electron Kelvin-Helmholtz instability (Che & Zank, 2020; Huang et al., 2015), oblique tearing mode instability (Daughton et al., 2011; Liu et al., 2013), electron current shear instability (Che et al., 2011; Fujimoto & Sydora, 2021), and lower-hybrid drift instability (Price et al., 2016). However, the development of turbulence within the electron diffusion region (EDR) of magnetotail reconnection remains poorly understood. Moreover, a few case studies suggest that more energetic electrons could be produced inside the turbulent diffusion region than in the laminar diffusion region, indicating that the turbulence might promote the electron energization process inside the diffusion region (Ergun et al., 2020; Ergun et al., 2018; Li, Wang, Lu, et al., 2022; Lu et al., 2023; Oka et al., 2022; Qi et al., 2024). However, the relationship between turbulence intensity and electron energization remains unclear, and a statistical or multi-case analysis is needed to explore how turbulence develops and influences the particle energization process in the reconnection diffusion region.

In this study, we analyze observations of 16 reconnection diffusion regions around the X-line. We systematically investigate the plasma conditions, electron energization, and turbulence properties within diffusion regions with varying turbulence intensities, aiming to shed light on the development of turbulence and its role in electron energization within the reconnection diffusion region.

2. Data Set and Criteria for Case Selection

All the data used in this paper are collected by the Magnetospheric Multiscale (MMS) mission. The direct current (DC) magnetic field data are measured by Flux Gate Magnetometer (FGM) with a time resolution of 16 Hz in survey mode and 128 Hz in the burst mode (Russell et al., 2016). The alternating current (AC) magnetic field data are obtained from Search-Coil Magnetometer (SCM) at 8,192 samples per second in burst mode (Le Contel et al., 2016). The electric field data are measured by the electric field double probe (EDP) with a time resolution of 128 Hz in survey mode and 8,192 Hz in burst mode (Ergun et al., 2016; Lindqvist et al., 2016). Energetic electron data are obtained from Fly's Eye Energetic Particle Spectrometer (FEEPs), in which the time resolution is 150 ms for electrons in burst mode (Blake et al., 2016; Mauk et al., 2016). The electron and ion moments data are taken from Fast Plasma Investigation (FPI), and the time resolution is 30 ms (4.5 s) for electrons and 150 ms (4.5 s) for ions in burst (survey) mode (Pollock et al., 2016). In the magnetotail, FPI measurements of both electrons and ions have known limitations. For electrons, extremely low densities can degrade full-moment estimates; therefore, we use partial-moment products for all electron moment data, which are designed to improve reliability in low-density environments such as the lobes. For ions, the dominant issue is the presence of substantial high-energy populations (>30 keV) outside the FPI energy range, which introduces large uncertainties in the derived ion moments. Consequently, ion moment data are excluded from our statistical analysis.

We examine the data measured in the magnetotail current sheet from 01 May 2017 to 01 October 2022, and identify the reconnecting current sheets based on the visual inspection of the data from MMS1. The search process is performed in the Geocentric Solar Ecliptic (GSE) coordinate system. This study mainly focuses on the diffusion region near the X-line (inside or near the EDR) with the following selection criteria: (a) a bipolar signature in the ion bulk flow $\mathbf{V}_{i,x}$; (b) a corresponding reversal of reconnected magnetic field $\mathbf{B}_z$; (c) small magnitude of magnetic field $\mathbf{B}_x$ and enhancements of current density around the reversal point of the $\mathbf{V}_{i,x}$. The time interval of each diffusion region around the X-line is defined as the period between the maximum $|\mathbf{V}_{i,x}|$ values on both sides of the

Table 1
Summary of the 16 Reconnection Events Analyzed in This Study

Case Num.	Interval (X-line)	B_{lobe} [nT]	T_{e0} [eV]
01	2017-07-11/22:33:30–22:34:30	14.4	798.9
02	2018-08-27/12:15:15–12:16:15	16.8	853.4
03	2017-05-28/03:58:00–03:59:00	21.4	1,755.3
04	2017-06-05/17:19:30–17:21:00	25.4	337.0
05	2017-06-19/09:40:00–09:46:00	19.5	1,040.5
06	2017-07-03/05:26:52–05:27:20	26.4	226.2
07	2017-07-06/15:46:20–15:47:40	19.1	306.0
08	2017-07-26/00:03:45–00:04:05	21.9	1,146.3
09	2017-07-26/07:28:00–07:29:15	18.6	1,196.8
10	2017-08-10/12:18:00–12:19:00	23.9	715.0
11	2018-08-27/11:40:50–11:42:05	18.7	853.5
12	2019-09-06/04:38:40–04:39:20	12.2	588.9
13	2020-08-02/16:55:00–17:15:00	14.9	785.5
14	2020-08-03/01:07:30–01:08:30	19.2	690.0
15	2020-08-26/23:00:40–23:01:40	19.9	304.1
16	2022-07-11/12:12:30–12:14:00	32.4	390.0

Note. Each row lists the event number, time interval around the X-line crossing, the root-mean-square magnetic fluctuation (δB_{rms}), the estimated lobe magnetic field strength (B_{lobe}), and background electron temperature. Some of them were first reported by previous studies. Case 1: (Torbert et al., 2018); Case 2: (Tang et al., 2022); Case 3: (X. Li, Wang, Lu, et al., 2022); Case 5: (Zhou, Man, et al., 2019); Case 6: (Chen et al., 2019); Case 7: (Shan Wang et al., 2019); Case 9: (R. E. Ergun et al., 2018); Case 10: (Zhou, Deng, et al., 2019); Case 11: (W. Y. Li et al., 2021); Case 12: (Qi et al., 2024); Some of these events can also be found in the event list of another statistical study (Shan Wang et al., 2022).

X-line. Moreover, we also exclude events lacking burst-mode data. Finally, a total of 16 diffusion regions near the X-line are identified and listed in Table 1.

3. Case Study

Figure 1 shows three diffusion regions in the burst mode data. For each case, panels (a–h) present: (a) electron energy spectrograms, (b) plasma density and plasma beta, (c) magnetic field components, (d) ion bulk velocity, (e) electron bulk velocity, (f) current density magnitude, (g) magnetic field fluctuations δB, and (h) electron temperature (parallel and perpendicular). Cases 1 and 2 are displayed in the local current coordinate system (LMN). In case 1, the LMN coordinate system is $L = (0.971, 0.216, −0.106)$, $M = (−0.234, 0.948, −0.215)$, $N = (0.054, 0.233, 0.971)$ in GSE coordinate, consistent with those in Torbert et al. (2018). The LMN coordinate system in case 2 is derived from R. E Ergun et al. (2022), where $L = (0.910, −0.385, −0.155)$, $M = (0.415, 0.848, 0.331)$, $N = (0.004, −0.365, 0.931)$. The signal in Case 3 is sufficiently clear in GSE coordinates, making transformation unnecessary, as also noted in previous studies (X Li, Wang, Lu, et al., 2022).

In case 1, the ion bulk flow velocity $\mathbf{V}_{i,L}$ changes from tailward to earthward (Figure 1d1), accompanied by the reversal of the reconnected magnetic field $\mathbf{B}_N$ from negative to positive (Figure 1c1), indicating that a retreating X-line is observed. At ~22:34:03 UT, when the $\mathbf{V}_{i,L}$ and $\mathbf{B}_N$ reverse, the magnetic field $\mathbf{B}_L$ is weak and the current density increases clearly (Figure 1f1), suggesting that the MMS crosses a reconnecting current sheet close to the X-line. Namely, the EDR is encountered by the MMS (Torbert et al., 2018). The enhanced current density displays a single peak (Figure 1e1), suggesting that the current sheet is an intact and quasi-laminar current layer.

In case 2, a retreating X-line is also observed, but with a large retreating speed of ~−200 km/s (Ergun et al., 2022; Tang et al., 2022). At around the reversal point of $\mathbf{V}_{i,L}$ (Figure 1d2, relative to the retreat speed ~−200 km/s), the magnetic field $\mathbf{B}_L$ changes from negative to positive (Figure 1c2), and a clear enhancement of current density is observed (Figure 1f2), indicating that the MMS encounters the EDR as well. Compared to case 1, the current structure here is more complex, with several current peaks around the center of the current sheet (Figure 1e2), suggesting the development of turbulence.

In case 3, current density enhancements (Figure 1f3) are also observed around the X-line region, where the ion outflow $\mathbf{V}_{i,X}$ (Figure 1c3) changes from tailward to earthward (Li, Wang, Lu, et al., 2022). However, unlike cases 1 and 2, the current density profile does not display a coherent current-layer structure. Instead, numerous current spikes are observed (Figure 1e3), suggesting that the development of the turbulence has broken the current sheet into a large number of fragmented currents. These fragmented structures likely form a three-dimensional network within the original sheet, indicating that turbulence has fully developed (Li, Wang, Huang, et al., 2022; Li, Wang, Lu, et al., 2022). Non-ideal electric fields are generated inside this fragmented current network (see Supporting Information S1). Moreover, although a density peak is present at the center of the diffusion region (Figure 3b), the overall density is significantly reduced compared to the plasma sheet (a zoomed-out view is provided in the Supporting Information S1). At the same time, the electron temperature is clearly enhanced. In combination, these observations indicate that case 3 represents an active lobe reconnection event, and the diffusion region has fully developed into a turbulent state.

The current sheet structures observed in these three cases can reflect the corresponding turbulence levels within the diffusion region. In the quasi-laminar region (weak turbulence), the current sheet remains an intact current layer (e.g., Case 1). As turbulence develops, the current layer becomes more complex. With moderate turbulence, the current sheet fragments into multiple sublayers (e.g., Case 2). With stronger turbulence, the current sheet further fragments into numerous smaller current structures, forming a filamentary current network (e.g., Case 3).
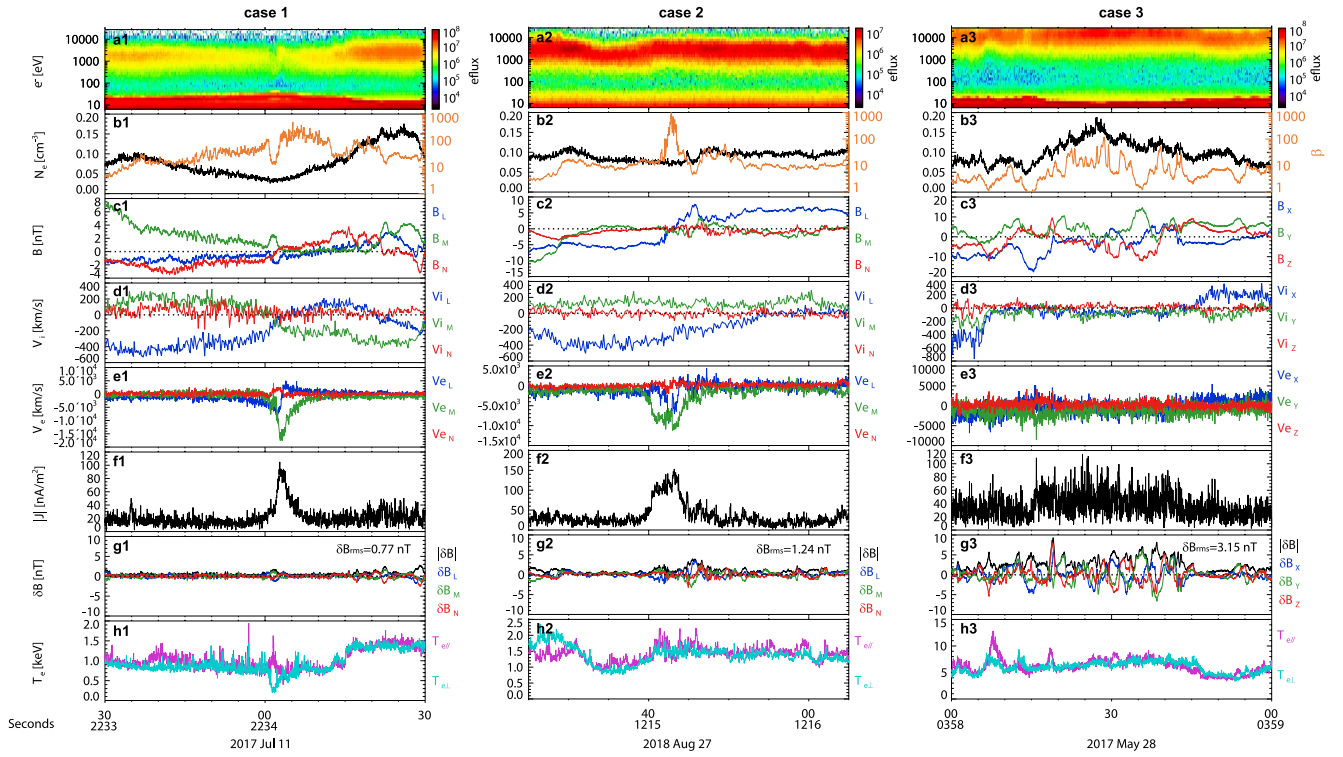
Figure 1. Three typical diffusion region cases with different turbulence intensities. (a) Electron omnidirectional spectrogram. (b) Number density (black trace) and plasma beta (yellow trace) (c) Magnetic field. (d) The ion bulk flows. (e) The electron bulk flows. (f) Current density. (g) Disturbance magnetic field with 5s detrending. (h) Electron temperature.

The perturbed magnetic field is always used to represent the turbulence intensity (Che et al., 2011; Ergun et al., 2022). In this study, to quantify the complexity of current structures (or the intensity of turbulence) inside the diffusion region, we calculate the root-mean-square of the disturbance magnetic field inside the diffusion region:

$$\delta B_{\text{rms}} = \sqrt{\langle \delta \boldsymbol{B} \cdot \delta \boldsymbol{B} \rangle_{\text{DR}}}$$

where $\delta \boldsymbol{B} = \boldsymbol{B} - \langle \boldsymbol{B} \rangle_{5s}$ is the perturbations magnetic field with 5s detrending, and $\langle \cdots \rangle_{\text{DR}}$ represents the average value over the diffusion region around the X-line (the durations are defined as the time interval between the peak values of the bidirectional ion jets, as shown in Table 1). The values of δB_{rms} effectively characterize the complexity of current structures (or the turbulence intensity). For example, in the three cases discussed above, δB_{rms} values are 0.77, 1.24, and 3.15 nT, corresponding to three different types of diffusion regions: quasi-laminar, moderately turbulent, and strongly turbulent, respectively.

It should be noted that δB_{rms} depends on the size of the detrending window, which is set to 5s in this work to remove the background fluctuations larger than the ion-scale (the average ion gyrofrequency in these cases is about 0.1 Hz). Moreover, to enable comparison across different cases, we normalize the δB_{rms} by the lobe magnetic field strength B_{lobe}. Here, B_{lobe} is determined from the pressure balance by averaging the total pressure inside the diffusion region and assuming negligible thermal pressure in the lobes. In the following sections, we use $\delta B_{\text{rms}}/B_{\text{lobe}}$ to denote the turbulence intensity inside the diffusion regions, and investigate the plasma conditions, energetic electrons, and turbulence properties inside the diffusion regions with different turbulence intensities.

4. Multi-Case Analysis

Figure 2 shows the plasma conditions inside the diffusion regions as listed in Table 1, and the colors of the data points are proportional to the plasma density. The average plasma number density inside the diffusion region is anti-correlated to the $\delta B_{\text{rms}}/B_{\text{lobe}}$ (Figure 2a), suggesting that the lower-density diffusion regions tend to exhibit
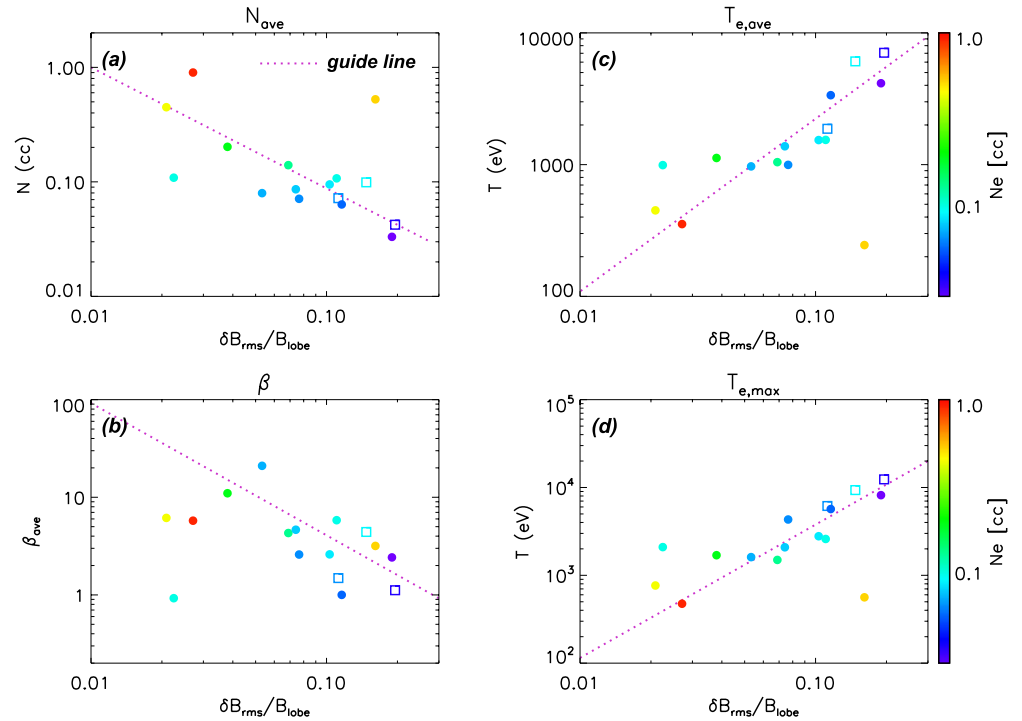
Figure 2. Plasma conditions in the diffusion region with different turbulence intensities. (a) Average number density at different root-mean-squares of the disturbance magnetic field $\delta B_{rms}/B_{lobe}$. (b) Average plasma beta at different $\delta B_{rms}/B_{lobe}$. (c) Average electron temperature at different $\delta B_{rms}/B_{lobe}$. (d) Maximum electron temperature at different $\delta B_{rms}/B_{lobe}$. The magenta lines in each panel serve as a guiding line and not a fitting. Events with current enhancement but disrupted current-layer structure are marked by squares. The color denotes electron density. These markers and colors are used consistently in the subsequent figures.

stronger turbulence. Since plasma density is important for understanding the development of turbulence during magnetotail reconnection, it is shown in color in the plots. In addition, different symbols are used to distinguish diffusion region types: regions with a coherent current-layer structure (e.g., Cases 1 and 2) are shown as circles, while those consisting of multiple filamentary currents (Case 3, Case 9, and Case 13) are marked by squares. This convention is applied consistently in all subsequent figures.

A negative correlation is also established between the average plasma beta and the $\delta B_{rms}/B_{lobe}$ (Figure 2b). Namely, lower plasma beta is associated with higher turbulence intensity. Figures 2c and 2d show the relationships between electron temperature (average temperature (Figure 2c) and maximum temperature
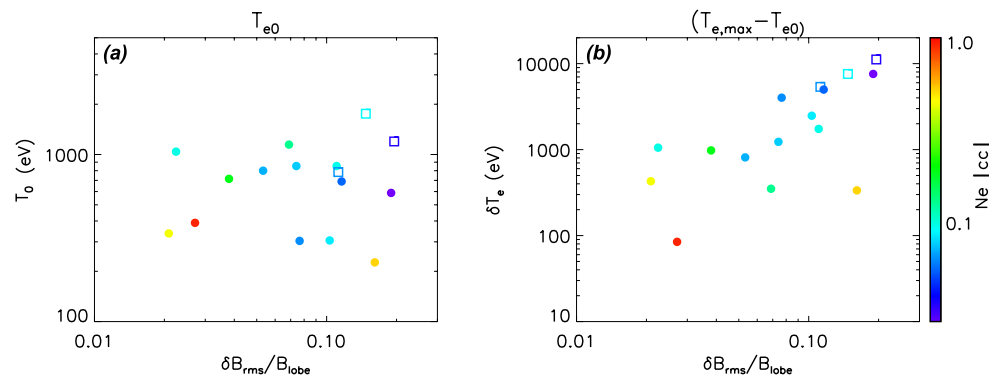

Figure 3. Electron temperature change in the diffusion region with different turbulence intensities. (a) Inflow region electron temperature T_{e0} at different $\delta B_{rms}/B_{lobe}$. (b) Temperature change between inflow region and maximum values ($T_{e,max} - T_{e,0}$) inside the diffusion region at different $\delta B_{rms}/B_{lobe}$.
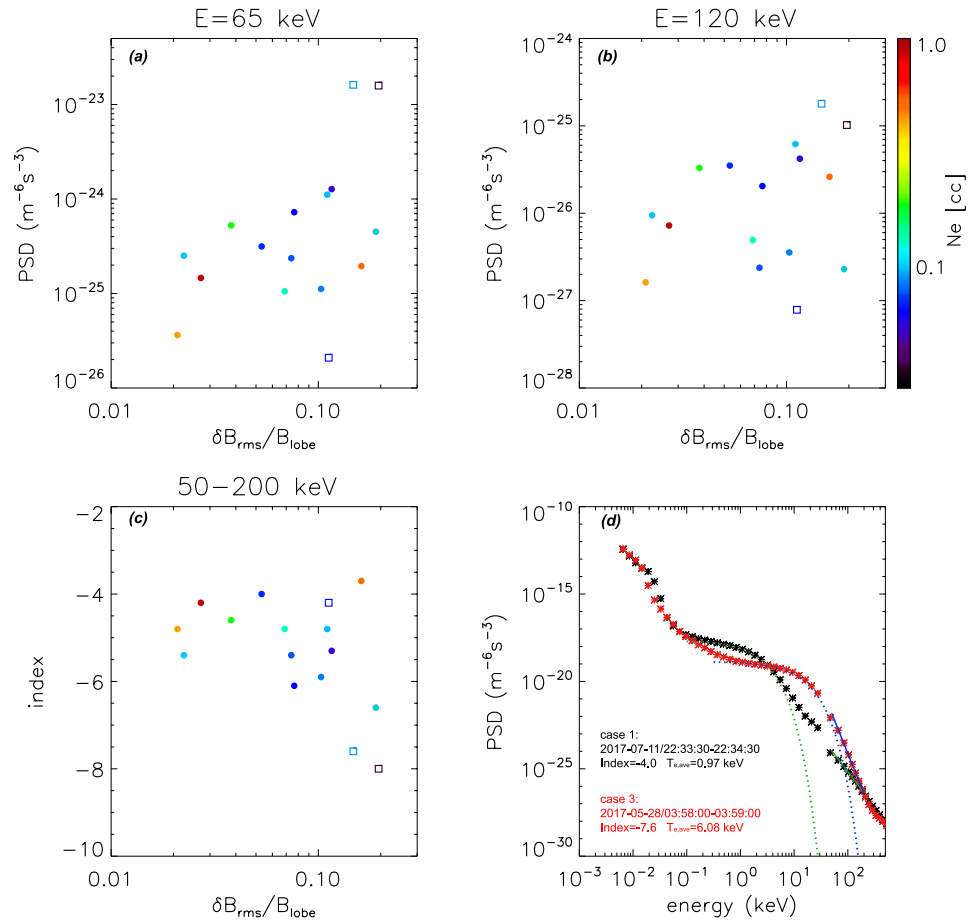
Figure 4. Energetic electrons in the diffusion region with different turbulence intensities. (a, b) the relations between $\delta B_{rms}/B_{lobe}$ and energetic electrons' phase space densities (PSDs) at energies of 65 and 120 keV. (c) The relations between $\delta B_{rms}/B_{lobe}$ and power-law indices of energetic electrons (50–200 keV). (d) The electron PSDs for case 1 and case 3. The dashed lines represent the Maxwellian fits for the thermal electrons (green dashed line for case 1, blue dashed line for case 3), and the solid lines represent the power-law fits for the non-thermal electrons (green solid line for case 1, blue solid line for case 3).

(Figure 2d)) and $\delta B_{rms}/B_{lobe}$. Both the average and maximum electron temperatures increase with the increase of $\delta B_{rms}/B_{lobe}$. This trend indicates that electron heating is likely enhanced in diffusion regions with stronger turbulence.

Alternatively, this trend may also be influenced by variations in the inflow temperature. To account for this effect, we obtain the inflow electron temperature (T_{e0}) for each event; for events without a direct inflow crossing, we use the temperature from an adjacent current-sheet crossing as a proxy (Table 1). As shown in Figure 3b, the positive relationship is observed between ($T_{e,max} - T_{e0}$) and $\delta B_{rms}/B_{lobe}$, demonstrating that the higher electron temperatures observed in strongly turbulent diffusion regions are primarily driven by turbulence-enhanced heating, rather than by hotter inflow electrons. The relationship between T_{e0} and $\delta B_{rms}/B_{lobe}$ is relatively weak (Figure 3a), which may result from our method of determining T_{e0} and the possible overestimation of T_{e0} in some cases, where the T_{e0} is taken from an adjacent current-sheet crossing. Nevertheless, it is worth noting that the range of T_{e0} is relatively small (0.2–2 keV), whereas most $T_{e,max}$ values fall within 1–10 keV. Therefore, even if T_{e0} is slightly overestimated, it does not significantly affect our main conclusion that ($T_{e,max} - T_{e0}$) increases with the turbulence level (Figure 3b).

The energetic electrons in the diffusion region are also studied in this work, with each diffusion region represented by an average of its electron phase space density (PSD) distribution. Figures 4a and 4b show the relations between $\delta B_{rms}/B_{lobe}$ and energetic electrons' PSDs at energies of 65 and 120 keV, respectively. A positive correlation is
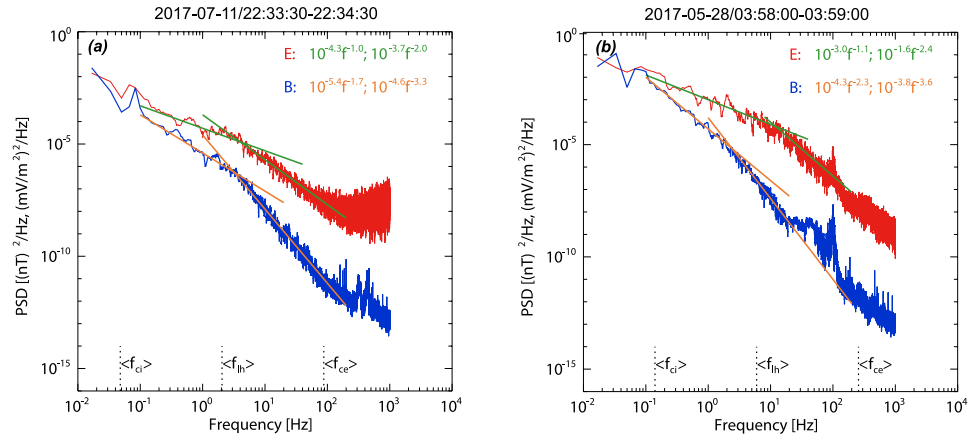
Figure 5. Example of magnetic and electric field power spectral density. (a, b) PSDs of the magnetic field and electric field for case 1 and case 3.

observed between $\delta B_{rms}/B_{lobe}$ and PSDs at each energy channel. Given that the number density is anti-correlated to the $\delta B_{rms}/B_{lobe}$, it should be concluded that the energetic electrons could be more easily generated in the diffusion region with stronger turbulence intensity. Figure 4c shows the relationship between $\delta B_{rms}/B_{lobe}$ and the power-law indices, which are obtained by fitting the power-law function to the PSD of energetic electrons (50–200 keV). The power-law indices become softer as the $\delta B_{rms}/B_{lobe}$ increases.

Finally, to study the turbulence properties of the diffusion regions, we calculate the power spectral density (PSD) of both magnetic and electric fields using the Fast Fourier Transform (FFT) and apply a nine-point moving average in the frequency domain. The PSD of the magnetic field is derived by combining low-frequency FGM data (<2 Hz) and high-frequency SCM data (>2 Hz), and the PSD of the electric field is obtained from EDP data. Given that the spatial scales of diffusion regions are sub-ion scale, we just focus on the PSDs within the frequency range from ion gyrofrequency (f_{ci}) to electron gyrofrequency (f_{ce}).

Figures 5a and 5b show the PSDs for case 1 and case 3 as representative examples. Both the electric field and magnetic field PSDs follow the double power-law distribution, with a break (denoted by f_b) observed between f_{ci} and f_{ce}. This behavior is observed in all cases, except for the magnetic field PSD of Case 8, where the intense waves with a broadband frequency range are observed. Case 8 will be investigated in future works and is therefore not included in the following analysis of the spectral indices and the spectral break frequencies of the magnetic and electric fields.

Figures 6a–6d present the relationships between $\delta B_{rms}/B_{lobe}$ and the spectral indices of both the magnetic and electric fields in the low-frequency (<f_b) and high-frequency (>f_b) ranges. In the low-frequency range, the spectral indices of the magnetic field vary from −2.4 to −1.5, with an average value of about −1.9. In the high-frequency (>f_b) range, the indices range from −4.0 to −2.8, with an average of −3.3. For the electric field, the spectral indices are always shallower than those of the magnetic field. In the low-frequency range, the indices range from −1.4 to −0.5, and the average value is −0.9. In the high-frequency range, the indices range from −3.4 to −2.0 with an average value of −2.6. The magnetic spectra seem to steepen with increasing turbulence, whereas this trend is not evident in the electric field spectra.

Figure 7 explores the relationship between the magnetic spectral break frequency f_b and the normalized turbulence intensity $\delta B_{rms}/B_{lobe}$. In Figure 7a, a weak positive trend between f_b and $\delta B_{rms}/B_{lobe}$ is visible. Since the observed spectral breaks fall between the ion cyclotron frequency (f_{ci}) and the electron cyclotron frequency (f_{ci}), we test whether f_b is associated with any nearby characteristic plasma frequencies. Specifically, we normalized f_b by three characteristic plasma frequencies: the ion cyclotron frequency (f_{ci}), the lower-hybrid drift frequency (f_{lh}), and the ion plasma frequency (f_{pi}), as shown in Figures 7b–7d. In all three cases, the normalized break frequencies span nearly two orders of magnitude without clear clustering. This suggests that the spectral break is not uniquely associated with any of these characteristic frequencies. On the other hand, even after normalization, the break frequency still tends to increase with stronger turbulence, suggesting that the spectral break may be more closely related to the turbulence intensity than to any specific characteristic plasma frequency.
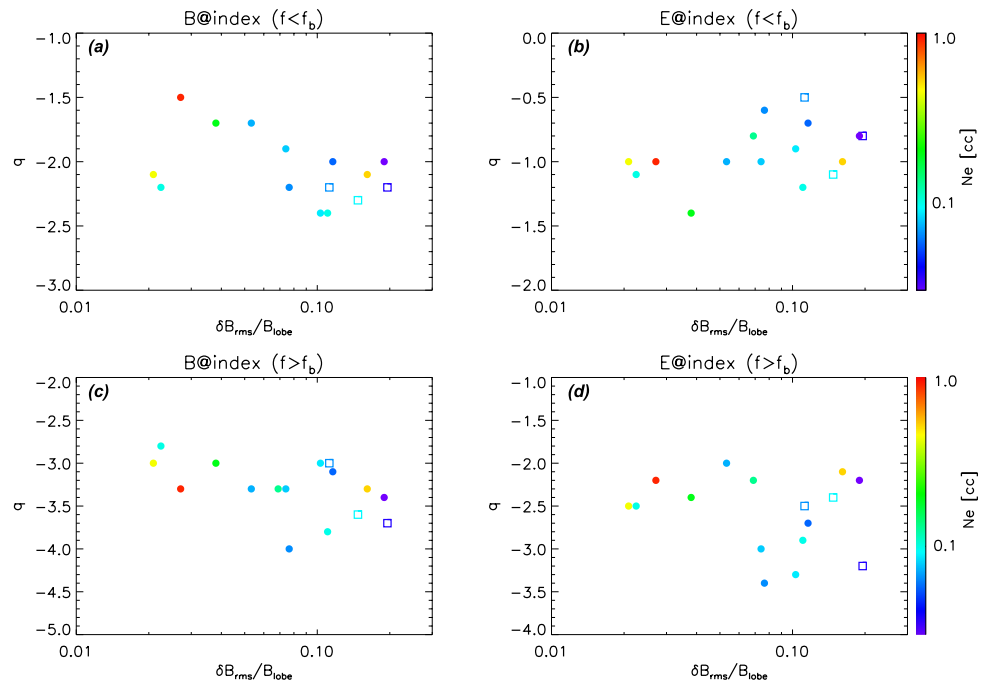
Figure 6. The relationships between $\delta B_{rms}/B_{lobe}$ and spectral indices of both the magnetic and electric fields. (a, c) show the magnetic field spectral indices in the low- ($<f_b$) and high-frequency ($>f_b$) ranges, respectively, while (b, d) show the electric field spectral indices in the corresponding frequency ranges.

Similarly, Figure 8 examines the relationship between the electric field spectral break frequency and the $\delta B_{rms}/B_{lobe}$. As shown in Figure 8a, a weak increasing trend is also observed, similar to the trend found in the magnetic field. The normalized break frequencies, shown in Figures 8b–8d, remain widely scattered across nearly two orders of magnitude, again showing no clear clustering around the characteristic plasma frequencies. Compared to the magnetic field, the break frequencies in the electric field spectra tend to appear at slightly higher values, suggesting that the two fields may reflect different aspects of the turbulent cascade or respond differently to small-scale dynamics.

5. Discussion and Conclusions

Generally, reconnection in the terrestrial magnetotail current sheet is thought to initiate within the plasma sheet, characterized by dense plasma. As reconnection progresses, the dense plasma is gradually depleted, and the tenuous lobe plasma starts to flow in (Baker et al., 2002; Ergun et al., 2022; Oka et al., 2022). This process is referred to as the transition from the plasma-sheet reconnection phase to the tail-lobe reconnection phase. In this work, we find that the turbulence intensity increases as the plasma density decreases inside the diffusion region, suggesting that the turbulence is more likely to develop and intensify in the diffusion region during the tail-lobe reconnection phase, where the plasma is more tenuous. Namely, the transition from plasma-sheet reconnection to tail-lobe reconnection should be accompanied by the development and intensification of turbulence, which may in turn accelerate the process of plasma depletion, facilitating the progression of this transition (Ergun et al., 2020; Lu et al., 2025; Sega & Ergun, 2024). Moreover, in the low-density conditions, the characteristic Alfven speed is higher for a given magnetic field strength, resulting in faster reconnection-related flows and stronger velocity shears, which are more susceptible to instability and the development of turbulence (Carter et al., 2001; Daughton et al., 2011).

In parallel, our observations also reveal an anti-correlation between plasma beta and the turbulence intensity inside the reconnection diffusion region. Since plasma beta also tends to decrease with decreasing density (even though the temperature may increase), this relationship may similarly reflect the plasma sheet to tail-lobe transition. On the other hand, low plasma beta conditions themselves may inherently strengthen turbulence development. In such conditions, where magnetic pressure exceeds plasma pressure, the current sheet tends to thin
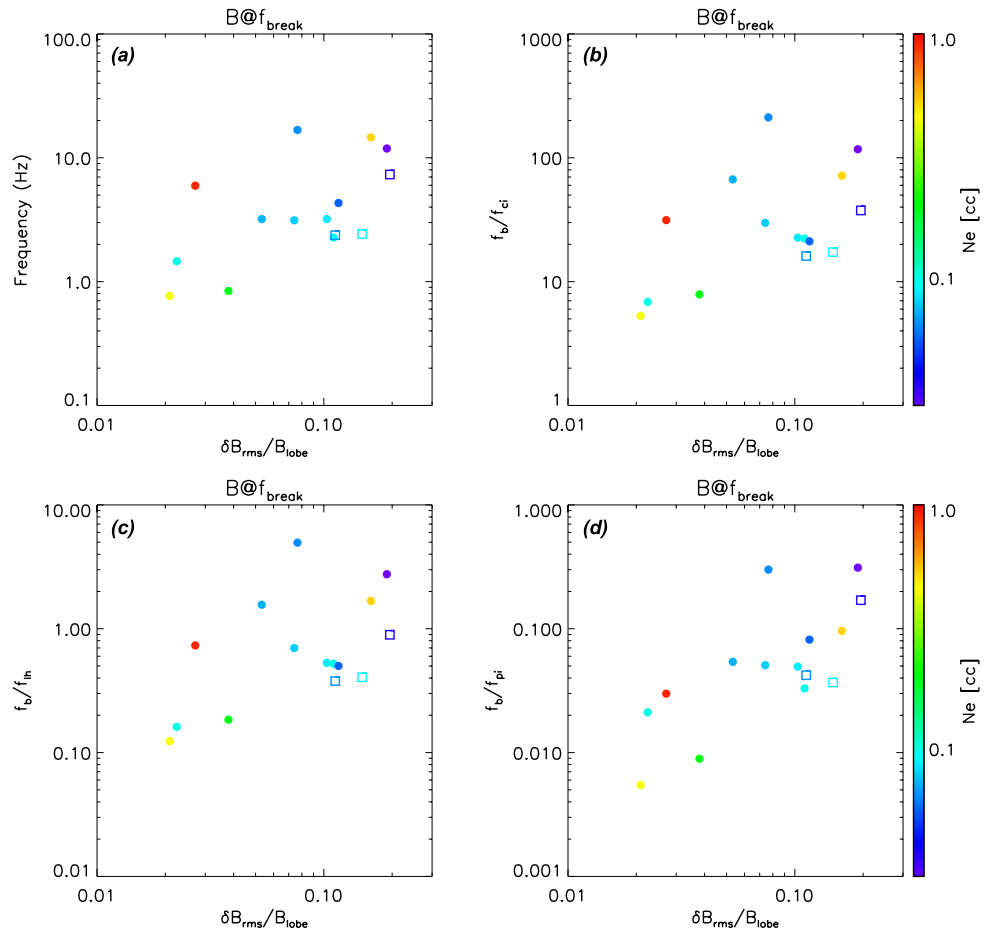
Figure 7. The relationship between the magnetic spectral break frequency and turbulence intensity. (a) Break frequency without normalization. (b–d) Break frequency normalized by the ion cyclotron frequency (f_{ci}), the lower-hybrid drift frequency (f_{lh}), and the ion plasma frequency (f_{pi}), respectively.

more readily, enhancing the growth of various instabilities such as tearing modes, lower-hybrid drift waves, and other current-driven turbulence, thereby facilitating the development of turbulence inside the reconnecting current sheet (Daughton et al., 2011; Schoeffler et al., 2011; Stawarz et al., 2024; Yoon et al., 2024).

It remains unclear whether plasma density or plasma beta plays the dominant role in driving turbulence. Since both of them decrease during the transition from plasma sheet to tail-lobe reconnection and are theoretically linked to turbulence generation, their effects are difficult to separate. Our data set of 16 events does not allow independent control of these variables. Future studies, particularly using simulations or larger observational samples, are needed to clarify their individual contributions.

A positive correlation between the energetic electron fluxes and turbulence intensity is established, indicating that the turbulence could effectively enhance electron energization within the diffusion region. However, contrary to the general understanding that the power-law index typically hardens as electrons are gradually accelerated, we find that with the increasing turbulence strength and the production of more energetic electrons, the power-law indices of the energetic electron population become softer. A similar trend has also been reported in a recent case study paper (Oka et al., 2022). One possible explanation is that in turbulent diffusion regions, stochastic scattering broadens the energy distribution leading to an increase in the thermal electron population. Our observations show that both the electron temperature and its enhancements are higher in the diffusion region with stronger turbulence (Figures 2c, 2d and 3), suggesting that the energy conversion process is primarily manifested as heating rather than direct acceleration inside the diffusion region with strong turbulence.
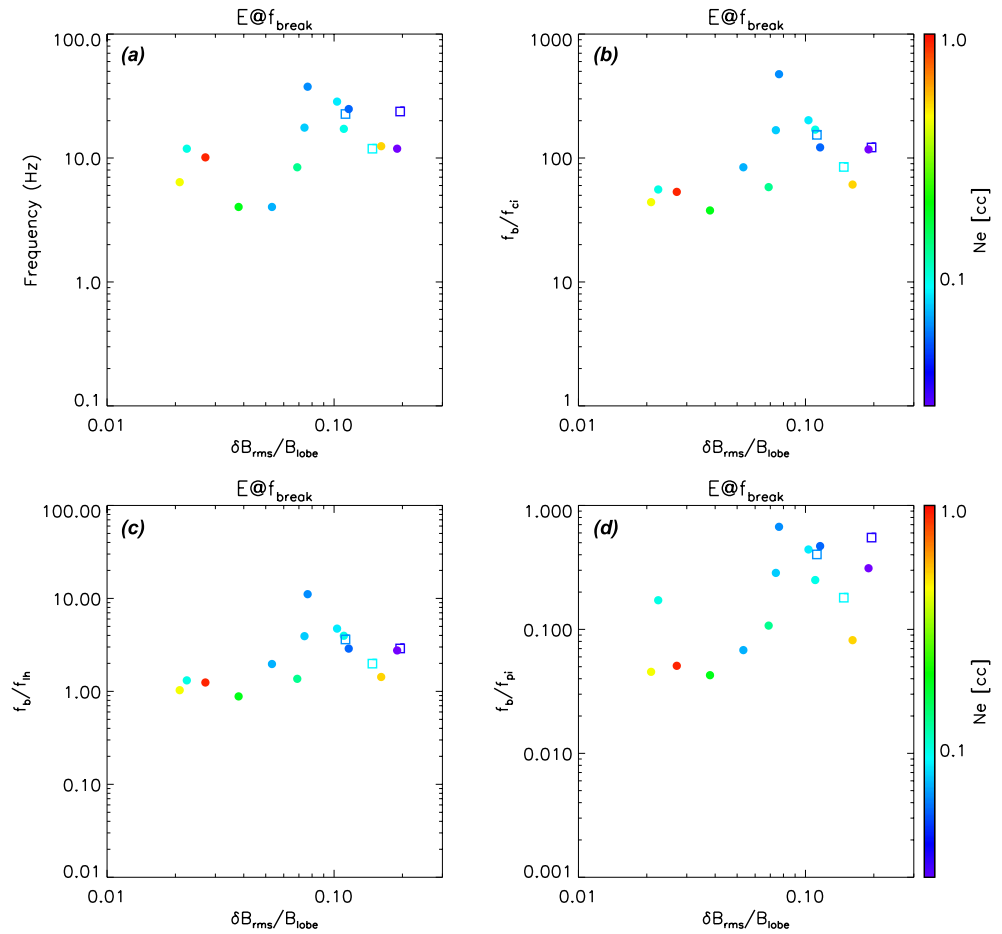
Figure 8. Relationship between electric spectral break frequency and turbulence intensity. The format is the same as in Figure 7.

For instance, Figure 4d compares the electron phase space densities (PSDs) in Case 1 (a quasi-laminar diffusion region, with an electron temperature of approximately 0.97 keV) and Case 3 (a strongly turbulent diffusion region, with an electron temperature of 6.0 keV). The higher temperature in Case 3 broadens the energy distribution and results in the enhancement of the energetic electron flux. But the power-law index is softer in Case 3 than in Case 1. This finding aligns with a previous study about the relationship between energetic electron fluxes and power-law indices in the magnetotail reconnection (Zhou et al., 2016). Combining the relationships between turbulence intensity and energetic electron flux, power law index, and temperature, it should be concluded that strong turbulence could effectively enhance electron energization inside the diffusion region, primarily through electron heating rather than direct acceleration.

To further understand the nature of turbulence within the reconnection diffusion regions, we analyze the PSDs of both magnetic and electric fields across the frequency range from ion gyrofrequency (f_{ci}) to the electron gyrofrequency (f_{ce}). The PSDs consistently exhibit a double power-law distribution with a spectral break occurring between f_{ci} and f_{ce}, which is consistent with previous case study observations and simulation results of the kinetic-scale turbulent reconnection (Ergun et al., 2020; Ergun et al., 2018; Li, Wang, Lu, et al., 2022; Lu et al., 2023; Wang et al., 2023).

The magnetic spectra tend to steepen with stronger turbulence, but such a trend is not obvious in the electric field spectra, indicating that understanding this relationship remains a complex problem. Moreover, previous simulation studies have shown that the spectral slopes can vary significantly across different evolution stages and spatial regions of reconnection (Adhikari et al., 2020; Daughton et al., 2014; Nakamura et al., 2021; Pucci

et al., 2017). A comprehensive simulation-based study will be necessary to fully understand the spectral indices during the evolution of reconnection, which we plan to pursue in future work.

The observed spectral break frequencies for both magnetic and electric field spectra consistently fall between the ion cyclotron frequency (f_{ci}) and the electron cyclotron frequency (f_{ce}). To examine the possible origin of these breaks, we tested whether they correspond to characteristic plasma frequencies, including f_{ci}, the lower-hybrid drift frequency (f_{lh}), and the ion plasma frequency (f_{pi}). However, after normalization, the break frequencies remain broadly scattered over nearly two orders of magnitude without clear clustering, suggesting that they are not uniquely associated with any of these characteristic plasma frequencies. Nevertheless, we note that the electric-field breaks tend to cluster around 1–$10 f_{lh}$, indicating that lower-hybrid drift waves may play a role in the development of turbulence inside the reconnection diffusion region. This is consistent with previous observations showing that lower-hybrid drift waves are frequently present in magnetotail reconnection diffusion regions (Chen et al., 2020; Shan Wang et al., 2022), suggesting their importance for both turbulence generation and dissipation. Moreover, the break frequency increases with turbulence intensity, and this positive trend remains evident even after normalization, indicating that the spectral break may be more closely governed by the turbulence strength itself.

As turbulence develops and intensifies inside the diffusion region, the diffusion region gradually breaks into smaller-scale fragmented currents. Since the energy dissipation in the turbulent diffusion region occurs within these fragmented currents (Che et al., 2011; Fu et al., 2017; Li, Wang, Lu, et al., 2022), the spatial scale of energy dissipation should also decrease as turbulence intensity increases. In our work, we find that the spectral break frequencies increase with the enhancement of the turbulence intensity. Given that the spectral breaks are often associated with the energy dissipation inside the turbulent plasma (Bourouaine et al., 2012; Dong et al., 2018, 2022; Perri, 2010), the observed increase in break frequency with stronger turbulence supports the idea that the current sheet gradually breaks up into smaller fragmented current structures as turbulence strengthens, and the energy dissipation occurs primarily inside these fragmented structures. However, because Taylor's frozen-in approximation (Taylor, 1938) is not valid in the reconnecting current sheet, the relationship between observed frequency and spatial scale is not straightforward, and this interpretation should be treated with caution. Nevertheless, the persistence of this trend even after normalizing the break frequencies by characteristic plasma frequencies suggests that this interpretation remains physically meaningful.

Magnetic islands (or magnetic flux ropes in 3D conditions) are widely regarded as essential structures in turbulent magnetic reconnection. When a reconnecting current sheet becomes sufficiently extended and unstable, multiple X-lines can develop, leading to the formation of a chain of magnetic islands (Daughton et al., 2010; Huang & Bhattacharjee, 2016). These islands grow, interact, and merge in a highly dynamic environment, promoting the development of turbulence and contributing to the breakdown of the current sheet into fragmented structures (Daughton et al., 2011; Nakamura et al., 2021; Wang et al., 2016). Moreover, the magnetic islands can trap and accelerate electrons to higher energies effectively (L. J. Chen et al., 2008; Drake et al., 2006; Fu et al., 2006; Lu et al., 2020), and facilitate the magnetic energy dissipation (Bergstedt et al., 2020; Li et al., 2023; Nakamura et al., 2021; Shimou Wang, Wang, et al., 2020) during the turbulent reconnection.

Several observational studies have reported the presence of magnetic islands within the reconnection diffusion regions (Hasegawa et al., 2022; Wang et al., 2010, 2023). However, not all turbulent diffusion regions exhibit clear signatures of magnetic islands or flux rope structures. In many cases (most of our events), only intermittent current structures or localized magnetic fluctuations are observed without island structures (Ergun et al., 2020; Li, Wang, Lu, et al., 2022). This discrepancy may result from several factors. One possibility is that the turbulence may be driven by other instabilities, such as the Kelvin–Helmholtz instability (Che & Zank, 2020; Huang et al., 2015), electron current shear instability (Che et al., 2011; Fujimoto & Sydora, 2021) or lower-hybrid drift instability (Price et al., 2016), which do not necessarily lead to island formation. Alternatively, it is also possible that the reconnecting current sheet has evolved into a fully developed turbulent state in which the magnetic island structures have broken up and are no longer distinguishable. These studies suggest that while magnetic islands play a prominent role in many turbulent reconnection scenarios, they are not a universal feature. Island-dominated reconnection represents only one possible manifestation of turbulent reconnection, which can arise through various mechanisms and take diverse structural forms.

In conclusion, we have analyzed the observations of 16 reconnection diffusion regions in the magnetotail current sheet. The results demonstrate that turbulence is more likely to develop in diffusion regions embedded in low-

density and low-beta plasma environments. Turbulence is associated with the enhanced electron energization, primarily manifesting as elevated electron temperatures. Moreover, the presence of spectral breaks between ion and electron cyclotron frequencies appears to be a robust feature of both magnetic and electric field fluctuations in reconnection diffusion regions, potentially reflecting energy dissipation mechanisms during turbulence reconnection.

Conflict of Interest

The authors declare no conflicts of interest relevant to this study.

Data Availability Statement

All the MMS data used in this work are available at the MMS data center (Magnetospheric Multiscale Science Data Center (MMS SDC), 2015). The data have been loaded, analyzed, and plotted using the SPEDAS software (Version 5.0) (Angelopoulos et al., 2019).

References

Adhikari, S., Shay, M., Parashar, T., Pyakurel, P. S., Matthaeus, W., Godzieba, D., et al. (2020). Reconnection from a turbulence perspective. *Physics of Plasmas*, *27*(4), 042305. https://doi.org/10.1063/1.5128376

Angelopoulos, V., Cruce, P., Drozdov, A., Grimes, E., Hatzigeorgiu, N., King, D., et al. (2019). The Space Physics Environment Data Analysis System (SPEDAS) [Software]. *Space Science Reviews*, *215*, 1–46. https://doi.org/10.1007/s11214-018-0576-4

Baker, D. N., Peterson, W. K., Eriksson, S., Li, X., Blake, J. B., Burch, J. L., et al. (2002). Timing of magnetic reconnection initiation during a global magnetospheric substorm onset. *Geophysical Research Letters*, *29*(24). https://doi.org/10.1029/2002gl015539

Bergstedt, K., Ji, H., Jara-Almonte, J., Yoo, J., Ergun, R., & Chen, L. J. (2020). Statistical properties of magnetic structures and energy dissipation during turbulent reconnection in the Earth's magnetotail. *Geophysical Research Letters*, *47*(19), e2020GL088540. https://doi.org/10.1029/2020gl088540

Blake, J. B., Mauk, B. H., Baker, D. N., Carranza, P., Clemmons, J. H., Craft, J., et al. (2016). The Fly's Eye Energetic Particle Spectrometer (FEEPS) sensors for the Magnetospheric Multiscale (MMS) mission. *Space Science Reviews*, *199*(1–4), 309–329. https://doi.org/10.1007/s11214-015-0163-x

Bourouaine, S., Alexandrova, O., Marsch, E., & Maksimovic, M. (2012). On spectral breaks in the power spectra of magnetic fluctuations in fast solar wind between 0.3 and 0.9 AU. *The Astrophysical Journal*, *749*(2), 102. https://doi.org/10.1088/0004-637x/749/2/102

Burch, J. L., Torbert, R. B., Phan, T. D., Chen, L. J., Moore, T. E., Ergun, R. E., et al. (2016). Electron-scale measurements of magnetic reconnection in space. *Science*, *352*(6290), aaf2939. https://doi.org/10.1126/science.aaf2939

Carter, T., Ji, H., Trintchouk, F., Yamada, M., & Kulsrud, R. (2001). Measurement of lower-hybrid drift turbulence in a reconnecting current sheet. *Physical Review Letters*, *88*(1), 015001. https://doi.org/10.1103/physrevlett.88.015001

Che, H., Drake, J. F., & Swisdak, M. (2011). A current filamentation mechanism for breaking magnetic field lines during reconnection. *Nature*, *474*(7350), 184–187. https://doi.org/10.1038/nature10091

Che, H., & Zank, G. P. (2020). Electron acceleration from expanding magnetic vortices during reconnection with a guide field. *The Astrophysical Journal*, *889*(1), 11. https://doi.org/10.3847/1538-4357/ab5d3b

Chen, L. J., Bhattacharjee, A., Puhl-Quinn, P. A., Yang, H., Bessho, N., Imada, S., et al. (2008). Observation of energetic electrons within magnetic islands. *Nature Physics*, *4*(1), 19–23. https://doi.org/10.1038/nphys777

Chen, L. J., Wang, S., Hesse, M., Ergun, R., Moore, T., Giles, B., et al. (2019). Electron diffusion regions in magnetotail reconnection under varying guide fields. *Geophysical Research Letters*, *46*(12), 6230–6238. https://doi.org/10.1029/2019gl082393

Chen, L.-J., Wang, S., Le Contel, O., Rager, A., Hesse, M., Drake, J., et al. (2020). Lower-hybrid drift waves driving electron nongyrotropic heating and vortical flows in a magnetic reconnection layer. *Physical Review Letters*, *125*(2), 025103. https://doi.org/10.1103/physrevlett.125.025103

Cozzani, G., Khotyaintsev, Y., Graham, D., Egedal, J., André, M., Vaivads, A., et al. (2021). Structure of a perturbed magnetic reconnection electron diffusion region in the Earth's magnetotail. *Physical Review Letters*, *127*(21), 215101. https://doi.org/10.1103/PhysRevLett.127.215101

Daughton, W., Nakamura, T. K. M., Karimabadi, H., Roytershteyn, V., & Loring, B. (2014). Computing the reconnection rate in turbulent kinetic layers by using electron mixing to identify topology. *Physics of Plasmas*, *21*(5), 052307. https://doi.org/10.1063/1.4875730

Daughton, W., Roytershteyn, V., Karimabadi, H., Yin, L., Albright, B. J., Bergen, B., & Bowers, K. J. (2011). Role of electron physics in the development of turbulent magnetic reconnection in collisionless plasmas. *Nature Physics*, *7*(7), 539–542. https://doi.org/10.1038/Nphys1965

Daughton, W., Roytershteyn, V., Karimabadi, H., Yin, L., Albright, B. J., Gary, S. P., et al. (2010). Secondary Island formation in collisional and collisionless kinetic simulations of magnetic reconnection. *Modern Challenges in Nonlinear Plasma Physics: A Festschrift Honoring the Career of Dennis Papadopoulos*, *1320*, 144–159. https://doi.org/10.1063/1.3544319

Deng, X. H., & Matsumoto, H. (2001). Rapid magnetic reconnection in the Earth's magnetosphere mediated by whistler waves. *Nature*, *410*(6828), 557–560. https://doi.org/10.1038/35069018

Dong, C., Wang, L., Huang, Y.-M., Comisso, L., & Bhattacharjee, A. (2018). Role of the plasmoid instability in magnetohydrodynamic turbulence. *Physical Review Letters*, *121*(16), 165101. https://doi.org/10.1103/physrevlett.121.165101

Dong, C., Wang, L., Huang, Y.-M., Comisso, L., Sandstrom, T. A., & Bhattacharjee, A. (2022). Reconnection-driven energy cascade in magnetohydrodynamic turbulence. *Science Advances*, *8*(49), eabn7627. https://doi.org/10.1126/sciadv.abn7627

Drake, J. F., Swisdak, M., Che, H., & Shay, M. A. (2006). Electron acceleration from contracting magnetic islands during reconnection. *Nature*, *443*(7111), 553–556. https://doi.org/10.1038/nature05116

Ergun, R., Ahmadi, N., Kromyda, L., Schwartz, S., Chasapis, A., Hoilijoki, S., et al. (2020). Observations of particle acceleration in magnetic reconnection–driven turbulence. *The Astrophysical Journal*, *898*(2), 154. https://doi.org/10.3847/1538-4357/ab9ab6

Ergun, R. E., Goodrich, K. A., Wilder, V., Ahmadi, N., Holmes, J. C., Eriksson, S., et al. (2018). Magnetic reconnection, turbulence, and particle acceleration: Observations in the Earth's magnetotail. *Geophysical Research Letters*, *45*(8), 3338–3347. https://doi.org/10.1002/2018gl076993

Ergun, R. E., Pathak, N., Usanova, M. E., Qi, Y., Vo, T., Burch, J. L., et al. (2022). Observation of magnetic reconnection in a region of strong turbulence. *The Astrophysical Journal Letters*, *935*(1), L8. https://doi.org/10.3847/2041-8213/ac81d4

Ergun, R. E., Tucker, S., Westfall, J., Goodrich, K. A., Malaspina, D. M., Summers, D., et al. (2016). The axial double probe and fields signal processing for the MMS mission. *Space Science Reviews*, *199*(1–4), 167–188. https://doi.org/10.1007/s11214-014-0115-x

Fu, H. S., Vaivads, A., Khotyaintsev, Y. V., Andre, M., Cao, J. B., Olshevsky, V., et al. (2017). Intermittent energy dissipation by turbulent reconnection. *Geophysical Research Letters*, *44*(1), 37–43. https://doi.org/10.1002/2016gl071787

Fu, X. R., Lu, Q. M., & Wang, S. (2006). The process of electron acceleration during collisionless magnetic reconnection. *Physics of Plasmas*, *13*(1), 012309. https://doi.org/10.1063/1.2164808

Fujimoto, K., & Sydora, R. D. (2021). Electromagnetic turbulence in the electron current layer to drive magnetic reconnection. *The Astrophysical Journal Letters*, *909*(1), L15. https://doi.org/10.3847/2041-8213/abe877

Genestreti, K. J., Li, X., Liu, Y.-H., Burch, J. L., Torbert, R. B., Fuselier, S. A., et al. (2022). On the origin of "patchy" energy conversion in electron diffusion regions. *Physics of Plasmas*, *29*(8), 082107. https://doi.org/10.1063/5.0090275

Hasegawa, H., Denton, R. E., Nakamura, T., Genestreti, K. J., Phan, T. D., Nakamura, R., et al. (2022). Magnetic field annihilation in a magnetotail electron diffusion region with electron-scale magnetic island. *Journal of Geophysical Research: Space Physics*, *127*(7), e2022JA030408. https://doi.org/10.1029/2022ja030408

Hesse, M., Schindler, K., Birn, J., & Kuznetsova, M. (1999). The diffusion region in collisionless magnetic reconnection. *Physics of Plasmas*, *6*(5), 1781–1795. https://doi.org/10.1063/1.873436

Huang, C., Lu, Q., Guo, F., Wu, M., Du, A., & Wang, S. (2015). Magnetic islands formed due to the Kelvin-Helmholtz instability in the outflow region of collisionless magnetic reconnection. *Geophysical Research Letters*, *42*(18), 7282–7286. https://doi.org/10.1002/2015gl065690

Huang, Y.-M., & Bhattacharjee, A. (2016). Turbulent magnetohydrodynamic reconnection mediated by the plasmoid instability. *The Astrophysical Journal*, *818*(1), 20. https://doi.org/10.3847/0004-637x/818/1/20

Ji, H. T., Daughton, W., Jara-Almonte, J., Le, A., Stanier, A., & Yoo, J. (2022). Magnetic reconnection in the era of exascale computing and multiscale experiments. *Nature Reviews Physics*, *4*(4), 263–282. https://doi.org/10.1038/s42254-021-00419-x

Le Contel, O., Leroy, P., Roux, A., Coillot, C., Alison, D., Bouabdellah, A., et al. (2016). The search-coil magnetometer for MMS. *Space Science Reviews*, *199*(1–4), 257–282. https://doi.org/10.1007/s11214-014-0096-9

Li, D., Chen, Y., Dong, C., Wang, L., & Toth, G. (2023). Numerical study of magnetic island coalescence using magnetohydrodynamics with adaptively embedded particle-in-cell model. *AIP Advances*, *13*(1), 015126. https://doi.org/10.1063/5.0122087

Li, W. Y., Khotyaintsev, Y. V., Tang, B., Graham, D. B., Norgren, C., Vaivads, A., et al. (2021). Upper-hybrid waves driven by meandering electrons around magnetic reconnection X line. *Geophysical Research Letters*, *48*(16), e2021GL093164. https://doi.org/10.1029/2021GL093164

Li, X., Wang, R., Huang, C., Lu, Q., Lu, S., Burch, J., & Wang, S. (2022). Energy conversion and partition in plasma turbulence driven by magnetotail reconnection. *The Astrophysical Journal*, *936*(1), 34. https://doi.org/10.3847/1538-4357/ac84d7

Li, X., Wang, R., Lu, Q., Hwang, K. J., Zong, Q., Russell, C. T., & Wang, S. (2019). Observation of nongyrotropic electron distribution across the electron diffusion region in the magnetotail reconnection. *Geophysical Research Letters*, *46*(24), 14263–14273. https://doi.org/10.1029/2019gl085014

Li, X., Wang, R., Lu, Q., Russell, C. T., Lu, S., Cohen, I. J., et al. (2022). Three-dimensional network of filamentary currents and super-thermal electrons during magnetotail magnetic reconnection. *Nature Communications*, *13*(1), 3241. https://doi.org/10.1038/s41467-022-31025-9

Lindqvist, P. A., Olsson, G., Torbert, R. B., King, B., Granoff, M., Rau, D., et al. (2016). The spin-plane double probe electric field instrument for MMS. *Space Science Reviews*, *199*(1–4), 137–165. https://doi.org/10.1007/s11214-014-0116-9

Liu, Y.-H., Daughton, W., Karimabadi, H., Li, H., & Roytershteyn, V. (2013). Bifurcated structure of the electron diffusion region in three-dimensional magnetic reconnection. *Physical Review Letters*, *110*(26), 265004. https://doi.org/10.1103/physrevlett.110.265004

Lu, Q., Huang, C., Xie, J., Wang, R., Wu, M., Vaivads, A., & Wang, S. (2010). Features of separatrix regions in magnetic reconnection: Comparison of 2-D particle-in-cell simulations and cluster observations. *Journal of Geophysical Research*, *115*(A11). https://doi.org/10.1029/2010ja015713

Lu, Q., Shu, Y., Chang, C., Lu, S., & Wang, R. (2025). The rate of magnetic reconnection in non-steady state. *Science Bulletin*, *S2095–9273*, 00622-X.

Lu, Q. M., Fu, H. S., Wang, R. S., & Lu, S. (2022). Collisionless magnetic reconnection in the magnetosphere. *Chinese Physics B*, *31*(8), 089401. https://doi.org/10.1088/1674-1056/ac76ab

Lu, S., Artemyev, A., Angelopoulos, V., & Pritchett, P. (2020). Energetic electron acceleration by ion-scale magnetic islands in turbulent magnetic reconnection: Particle-in-cell simulations and ARTEMIS observations. *The Astrophysical Journal*, *896*(2), 105. https://doi.org/10.3847/1538-4357/ab908e

Lu, S., Lu, Q., Wang, R., Li, X., Gao, X., Huang, K., et al. (2023). Kinetic scale magnetic reconnection with a turbulent forcing: Particle-in-cell simulations. *The Astrophysical Journal*, *943*(2), 100. https://doi.org/10.3847/1538-4357/acaf7a

Ma, Z. W., & Bhattacharjee, A. (2001). Hall magnetohydrodynamic reconnection: The Geospace environment modeling challenge. *Journal of Geophysical Research: Space*, *106*(A3), 3773–3782. https://doi.org/10.1029/1999ja001004

Magnetospheric Multiscale Science Data Center (MMS SDC). (2015). Level-2/3 data products. Laboratory for atmospheric and space physics [Dataset]. *University of Colorado*. Retrieved from https://lasp.colorado.edu/mms/sdc/public/about/browse-wrapper/

Mauk, B. H., Blake, J. B., Baker, D. N., Clemmons, J. H., Reeves, G. D., Spence, H. E., et al. (2016). The Energetic Particle Detector (EPD) investigation and the Energetic Ion Spectrometer (EIS) for the Magnetospheric Multiscale (MMS) mission. *Space Science Reviews*, *199*(1–4), 471–514. https://doi.org/10.1007/s11214-014-0055-5

Nakamura, T., Hasegawa, H., Genestreti, K., Denton, R., Phan, T., Stawarz, J., et al. (2021). Fast cross-scale energy transfer during turbulent magnetic reconnection. *Geophysical Research Letters*, *48*(13), e2021GL093524. https://doi.org/10.1029/2021gl093524

Oieroset, M., Phan, T. D., Fujimoto, M., Lin, R. P., & Lepping, R. P. (2001). Detection of collisionless reconnection in the Earth's magnetotail. *Nature*, *412*(6845), 414–417. https://doi.org/10.1038/35086520

Oka, M., Phan, T., Øieroset, M., Turner, D., Drake, J., Li, X., et al. (2022). Electron energization and thermal to non-thermal energy partition during Earth's magnetotail reconnection. *Physics of Plasmas*, *29*(5), 052904. https://doi.org/10.1063/5.0085647

Perri, S., Carbone, V., & Veltri, P. (2010). Where does fluid-like turbulence break Down in the solar wind? *The Astrophysical Journal Letters*, *725*(1), L52–L55. https://doi.org/10.1088/2041-8205/725/1/l52

Pollock, C., Moore, T., Jacques, A., Burch, J., Gliese, U., Saito, Y., et al. (2016). Fast plasma investigation for Magnetospheric multiscale. *Space Science Reviews*, *199*(1–4), 331–406. https://doi.org/10.1007/s11214-016-0245-4

Price, L., Swisdak, M., Drake, J. F., Cassak, P. A., Dahlin, J. T., & Ergun, R. E. (2016). The effects of turbulence on three-dimensional magnetic reconnection at the magnetopause. *Geophysical Research Letters*, *43*(12), 6020–6027. https://doi.org/10.1002/2016gl069578

Pritchett, P. L. (2001). Collisionless magnetic reconnection in a three-dimensional open system. *Journal of Geophysical Research: Space*, *106*(A11), 25961–25977. https://doi.org/10.1029/2001ja000016

Pucci, F., Servidio, S., Sorriso-Valvo, L., Olshevsky, V., Matthaeus, W., Malara, F., et al. (2017). Properties of turbulence in the reconnection exhaust: Numerical simulations compared with observations. *The Astrophysical Journal*, *841*(1), 60. https://doi.org/10.3847/1538-4357/aa704f

Qi, Y., Ergun, R., Pathak, N., Phan, T. D., Burch, J. L., Chasapis, A., et al. (2024). Investigation of a magnetic reconnection event with extraordinarily high particle energization in magnetotail turbulence. *The Astrophysical Journal Letters*, *962*(2), L39. https://doi.org/10.3847/2041-8213/ad24eb

Russell, C. T., Anderson, B. J., Baumjohann, W., Bromund, K. R., Dearborn, D., Fischer, D., et al. (2016). The magnetospheric multiscale magnetometers. *Space Science Reviews*, *199*(1–4), 189–256. https://doi.org/10.1007/s11214-014-0057-3

Schoeffler, K. M., Drake, J., & Swisdak, M. (2011). The effects of plasma beta and anisotropy instabilities on the dynamics of reconnecting magnetic fields in the Heliosheath. *The Astrophysical Journal*, *743*(1), 70. https://doi.org/10.1088/0004-637x/743/1/70

Sega, D. D., & Ergun, R. E. (2024). Turbulent magnetic reconnection as an acceleration mechanism in Earth's magnetotail. *The Astrophysical Journal*, *965*(2), 129. https://doi.org/10.3847/1538-4357/ad3101

Shay, M., Phan, T., Haggerty, C., Fujimoto, M., Drake, J., Malakit, K., et al. (2016). Kinetic signatures of the region surrounding the X line in asymmetric (magnetopause) reconnection. *Geophysical Research Letters*, *43*(9), 4145–4154. https://doi.org/10.1002/2016gl069034

Shay, M. A., Drake, J. F., Denton, R. E., & Biskamp, D. (1998). Structure of the dissipation region during collisionless magnetic reconnection. *Journal of Geophysical Research*, *103*(A5), 9165–9176. https://doi.org/10.1029/97ja03528

Stawarz, J., Muñoz, P., Bessho, N., Bandyopadhyay, R., Nakamura, T., Eriksson, S., et al. (2024). The interplay between collisionless magnetic reconnection and turbulence. *Space Science Reviews*, *220*(8), 90. https://doi.org/10.1007/s11214-024-01124-8

Tang, B. B., Li, W. Y., Khotyaintsev, Y. V., Graham, D. B., Gao, C. H., Chen, Z. Z., et al. (2022). Fine structures of the electron current sheet in magnetotail guide-field reconnection. *Geophysical Research Letters*, *49*(9), e2021GL097573. https://doi.org/10.1029/2021GL097573

Taylor, G. I. (1938). The spectrum of turbulence. *Proceedings of the Royal Society of London—Series A: Mathematical and Physical Sciences*, *164*(919), 476–490. https://doi.org/10.1098/rspa.1938.0032

Torbert, R. B., Burch, J. L., Phan, T. D., Hesse, M., Argall, M. R., Shuster, J., et al. (2018). Electron-scale dynamics of the diffusion region during symmetric magnetic reconnection in space. *Science*, *362*(6421), 1391–1395. https://doi.org/10.1126/science.aat2998

Wang, L., Hakim, A. H., Bhattacharjee, A., & Germaschewski, K. (2015). Comparison of multi-fluid moment models with particle-in-cell simulations of collisionless magnetic reconnection. *Physics of Plasmas*, *22*(1), 012108. https://doi.org/10.1063/1.4906063

Wang, R. S., Lu, Q. M., Lu, S., Russell, C. T., Burch, J. L., Gershman, D. J., et al. (2020). Physical implication of two types of reconnection electron diffusion regions with and without ion-coupling in the magnetotail current sheet. *Geophysical Research Letters*, *47*(21), e2020GL088761. https://doi.org/10.1029/2020GL088761

Wang, R. S., Lu, Q. M., Du, A. M., & Wang, S. (2010). In situ observations of a secondary magnetic Island in an ion diffusion region and associated energetic electrons. *Physical Review Letters*, *104*(17), 175003. https://doi.org/10.1103/PhysRevLett.104.175003

Wang, R. S., Lu, Q. M., Nakamura, R., Huang, C., Du, A. M., Guo, F., et al. (2016). Coalescence of magnetic flux ropes in the ion diffusion region of magnetic reconnection. *Nature Physics*, *12*(3), 263–267. https://doi.org/10.1038/Nphys3578

Wang, R. S., Nakamura, R., Lu, Q., Baumjohann, W., Ergun, R., Burch, J., et al. (2017). Electron-scale quadrants of the Hall magnetic field observed by the magnetospheric multiscale spacecraft during asymmetric reconnection. *Physical Review Letters*, *118*(17), 175101. https://doi.org/10.1103/PhysRevLett.118.175101

Wang, R. S., Wang, S. M., Lu, Q. M., Li, X. M., Lu, S., & Gonzalez, W. (2023). Direct observation of turbulent magnetic reconnection in the solar wind. *Nature Astronomy*, *7*(1), 18–28. https://doi.org/10.1038/s41550-022-01818-5

Wang, S., Chen, L. J., Bessho, N., Hesse, M., Giles, B. L., & Moore, T. E. (2019). Ion behaviors in the reconnection diffusion region of a corrugated magnetotail current sheet. *Geophysical Research Letters*, *46*(10), 5014–5020. https://doi.org/10.1029/2019gl082226

Wang, S., Chen, L. J., Bessho, N., Ng, J., Hesse, M., Graham, D. B., et al. (2022). Lower-hybrid wave structures and interactions with electrons observed in magnetotail reconnection diffusion regions. *Journal of Geophysical Research: Space Physics*, *127*(5), e2021JA030109. https://doi.org/10.1029/2021ja030109

Wang, S., Wang, R., Lu, Q., Fu, H., & Wang, S. (2020). Direct evidence of secondary reconnection inside filamentary currents of magnetic flux ropes during magnetic reconnection. *Nature Communications*, *11*(1), 3964. https://doi.org/10.1038/s41467-020-17803-3

Webster, J. M., Burch, J. L., Reiff, P. H., Daou, A. G., Genestreti, K. J., Graham, D. B., et al. (2018). Magnetospheric multiscale dayside reconnection electron diffusion region events. *Journal of Geophysical Research: Space*, *123*(6), 4858–4878. https://doi.org/10.1029/2018ja025245

Yoon, Y. D., Moore, T. E., Wendel, D. E., Laishram, M., & Yun, G. S. (2024). Enablement or suppression of collisionless magnetic reconnection by the background plasma beta and guide field. *Geophysical Research Letters*, *51*(22), e2024GL112126. https://doi.org/10.1029/2024gl112126

Zenitani, S., Hesse, M., Klimas, A., & Kuznetsova, M. (2011). New measure of the dissipation region in collisionless magnetic reconnection. *Physical Review Letters*, *106*(19), 195003. https://doi.org/10.1103/PhysRevLett.106.195003

Zhou, M., Deng, X. H., Zhong, Z. H., Pang, Y., Tang, R. X., El-Alaoui, M., et al. (2019). Observations of an electron diffusion region in symmetric reconnection with weak guide field. *The Astrophysical Journal*, *870*(1), 34. https://doi.org/10.3847/1538-4357/aaf16f

Zhou, M., Li, T. M., Deng, X. H., Pang, Y., Xu, X. J., Tang, R. X., et al. (2016). Statistics of energetic electrons in the magnetotail reconnection. *Journal of Geophysical Research: Space*, *121*(4), 3108–3119. https://doi.org/10.1002/2015ja022085

Zhou, M., Man, H. Y., Zhong, Z. H., Deng, X. H., Pang, Y., Huang, S. Y., et al. (2019). Sub-ion-scale dynamics of the ion diffusion region in the magnetotail: MMS observations. *Journal of Geophysical Research: Space*, *124*(10), 7898–7911. https://doi.org/10.1029/2019ja026817